Inorganic Chemistry

Article

pubs.acs.org/IC

Structural and Relative Stabilities, Electronic Properties, and Hardness of Iron Tetraborides from First Prinicples

Li-Ping Ding,[†] Xiao-Yu Kuang,*[,†] Peng Shao,[†] and Xiao-Fen Huang[‡]

[†]Institute of Atomic and Molecular Physics, Sichuan University, Chengdu 610065, China

[‡]Physics Department, Sichuan Normal University, Chengdu 610068, China

Supporting Information

ABSTRACT: First-principles calculations were carried out to investigate the structure, phase stability, electronic property, and roles of metallicity in the hardness for recently synthesized FeB_4 with various different structures. Our calculation indicates that the orthorhombic phase with *Pnnm* symmetry is the most energetically stable one. The other four new dynamically stable phases belong to space groups monoclinic *C*2/*m*, orthorhombic *Pmmn*, trigonal $R\bar{3}m$, and hexagonal $P6_3/mmc$. Their mechanical and thermodynamic stabilities are verified by calculating elastic constants, formation enthalpies, and phonon dispersions. We found that all phases are stabilized further under pressure. Above the pressure of about 50 GPa, the formation enthalpy of *Pmmn* is almost equal to that of $P6_3/mmc$ phase. The analysis on density of states not only demonstrates that formation of strong covalent bonding in these compounds contributes greatly to their stabilities but also that they all exhibit metallic behavior which does not relate to the approach used. By considering metallic contributions, the estimated Vickers hardness values based on the semiempirical model show that the OsB_4-structured FeB_4, with a hardness of 48.1 GPa, well exceeding the limitation of superhardness (40 GPa), is more hard than the most stable phase. The others are predicted to be potential hard materials. Moreover, the atomic configuration and strong B−B covalent bonds are found to play important roles in the hardness of materials.

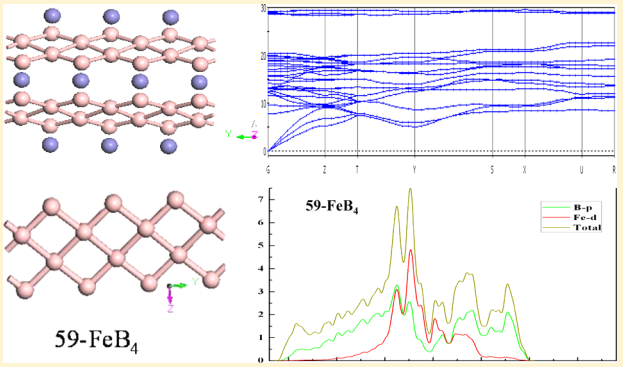

1. INTRODUCTION

Ultrahard and superhard materials are of considerable interest due to their excellent mechanical and thermal properties such as high hardness and melting point, larger strength, as well as wear resistance. In the past decades, a class of superhard materials (e.g., diamond,[1] cubic BN,[2] BC_2N,[3] B_6O,[4] and BC_5,[5] etc.) formed by a light element with a strong covalent bond has been generally accepted. However, diamond reacts with iron at moderately high temperature, and cubic-BN is quite expensive because of its harsh synthesis conditions. These limitations prevent them from being used as abrasive or cutting tools for ferrous metals. Therefore, great efforts have been devoted to search for new hard materials in place of diamond. Accordingly, another family of super- or ultrahard materials, including large electron-rich transition-metal (TM) boride, carbide, nitride, and oxide (e.g., PtN_2,[6] OsB_2,[7] ReB_2,[8,9] TaB_2,[10] and RuO_2,[11] etc.), has received considerable attention because they possess high bulk moduli. Although some of these superhard materials have been synthesized, there are some findings that strongly challenge the general idea to design an intrinsically superhard TM light element based only on its high bulk moduli.[7,8,12,13] For example, OsB_2 possesses high zero-pressure elastic moduli but low hardness due to the presence of Os−Os layers with weak metallic bonds.[13] ReB_2 was believed to be intrinsically superhard,[8] whereas its load-invariant hardness is less than 30 GPa.[14] In addition, the rhenium nitrides[15] with a large bulk modulus of about 400 GPa, under high temperature and pressure, have attracted much interest, while the Zhang group's[16] study showed that thermodynamic instability, relatively low shear moduli and strength, as well as relatively soft polar Re−N bonds inherently limit their hardness.

Recently, Gu et al.[17] synthesized tungsten tetraboride (WB_4) and measured its average hardness as high as 46.2 GPa, which is comparable to that (45−50 GPa) of cubic BN. On the basis of first-principles calculations, Wang et al.[18] explained the high hardness as a consequence of the three-dimensional (3D) boron network with strong covalent B_2 units and a planar boron sublattice in the hexagonal structure. On the basis of the global structural optimization, Li et al.[19] determined that the $P6_3/mmc$-2u WB_4 is the ground state structure of tungsten tetraboride. These above findings motivate researchers to synthesize tetraborides of transition metals by introducing more boron atoms to form a 3D boron network with strong covalent bonds.[17,20] In 2008, Wang et al. proposed that Osinium tetraboride (OsB_4) within the WB_4-type structure was a superhard material with a claimed hardness of 46.2 GPa,[18] but it has a much lower shear modulus of 52 GPa. Later, Zhang

Received: November 23, 2013
Published: March 7, 2014

   dx.doi.org/10.1021/ic402913k | *Inorg. Chem.* 2014, 53, 3471−3479

Table 1. Calculated Equilibrium Lattice Parameters, a (Å), b (Å), and c (Å), Cell Volumes per Formula Unit, V (Å^3), Densities and Difference in Total Energy for All Considered FeB_4 with a Various Different Structures, Along with the Available Experimental and Theoretical Values

	space	a	b	c	V	ρ	ΔE
58-FeB_4	$Pnnm$	4.483	5.253	3.000	35.810	4.66	0.00
exp.[a]		4.578(3)	5.298(3)	2.991(2)	36.376(8)		
theor.[b]		4.521	5.284	3.006	35.905		
theor.[c]		4.579	5.298	2.999			
12-FeB_4	$C2/m$	13.739	2.961	5.252	35.398	4.65	0.07
theor.[b]		13.961	2.936	5.316			
194-FeB_4	$P6_3/mmc$	5.162		6.044	34.863	4.72	2.58
71-FeB_4	$Immm$	4.483	5.257	3.040	35.821	4.59	0.11
theor.[b,d]		4.518	5.287	3.052	<36		
59-FeB_4	$Pmmn$	6.635	2.786	3.791	35.031	4.70	0.26
166-FeB_4	R-3m	2.863		14.988	35.471	4.64	0.40
RuB_4–FeB_4	$P6_3/mmc$	2.865		9.916	35.239	4.67	0.22

[a]Reference 32, experiment. [b]Reference 31, VASP. [c]Reference 44, VASP. [d]Reference 33, VASP.

et al.[21] proposed an orthorhombic $Pmmn$ structure for OsB_4, which is energetically much superior to the WB_4-type structure. These pioneering studies open up a novel route for the search of new superhard materials. To date, although many tetraborides of TM neighboring Fe (i.e., WB_4, CrB_4, OsB_4, etc.) have been synthesized and predicted, less is known about the boron-rich Fe–B compounds. Only a few reports are available: observation of a metastable FeB_{49} intercalation compound,[22] possible synthesis of amorphous[23] and the AlB_2-type[24] iron diborides. These modeling works have given insight into their binding, magnetic, and structural properties[25−30] but not systematically explored the possibility of obtaining new stable iron borides. Until 2010, Kolmogorow et al.[31] showed that $oP10$-FeB_4 is stabilized by the distortion of a 3D boron network and has potential for phonon-mediated superconductivity with a T_c of 15−20 K. Very recently, Gou et al.[32] synthesized orthorthombic $oP10$ (space group $Pnnm$) FeB_4 at pressures above 8 GPa and high temperatures. They found that it is highly incompressible with the nanoidentation hardness of 65(5) GPa, well exceeding the expectations about its potential mechanical properties.[33] This finding bridges the gap between the superhardness and superconductivity community and may lead to a possibility for designing new superconducting nanoelectromechanical systems or observation of new fundamental effects. Thus, characterization of the structural assignment, elastic property, and stability of newly synthesized FeB_4 is an important issue, which is essential to further study.

In this paper, we systematically explore the crystal structure, relatively stability, elastic property, formation enthalpy, and hardness of FeB_4 with various different structures. The aim of the present work is to give a comprehensive understanding of the stability and properties of FeB_4 and compare with previous experimental and calculated results.

2. COMPUTATIONAL METHODS

In this work, the experimentally determined structure orthorhombic $oP10$-FeB_4 (No. 58, $Pnnm$)[31] and theoretically proposed new structure monoclinic $mS30$-FeB_4 (No. 12, $C2/m$)[31] via an evolutionary algorithms (EAs) search were considered (designated as 58- and 12-FeB_4, respectively, hereafter). Apart from these two structures, another five possible structures were also adopted here. They are hexagonal $hP20$-WB_4 type (No. 194, $P6_3/mmc$, Z = 4),[34] orthorhombic $oI10$-CrB_4 (No. 71, $Immm$)[35] and OsB_4 (No. 59, $Pmmn$),[21] trigonal ReB_4 (No. 166, R-3m, Z = 3),[36] as well as hexagonal RuB_4 (No. 194, $P6_3/mmc$, Z = 2)[37] (denoted as 194-, 59-, 166-, and RuB_4–FeB_4, respectively, hereafter).

Geometry optimization was carried out using density functional theory within the CASTEP code.[38] The exchange-correlation functional was taken into account through the generalized gradient approximation of Perdew, Burke, and Ernzerhof (GGA-PBE).[39] Optimizations of the structural parameters and atomic positions were realized by minimizing the forces and stress tensors, and the interactions between the ions and the electrons of Fe and B were expressed by a Vanderbit ultrasoft pseudopotential.[40] The cutoff energy of the atomic wave functions was set to be 650 eV, and the Brillouin zone sampling is performed using the Monkhorst–Pack grid,[41] such as the 8 × 7 × 12, 7 × 6 × 11, and 6 × 15 × 11 grids for the respective orthorhombic $Pnnm$, $Immm$, and $Pmmn$ structures, a 2 × 11 × 6 grid for the $P6_3/mmc$ structure, a 13 × 13 × 2 grid for the trigonal R-3m structure, and a 13 × 13 × 4 grid for the hexagonal $P6_3/mmc$ structure. Within each self-consistency cycle, the total energy was converged to be within 1×10^{-6} eV.

To further confirm the mechanical stability of these FeB_4 with different structures, the elastic constants were calculated by the strain–stress method. The elastic stability of a given crystal should satisfy the generalized stability criteria.[42] The bulk modulus B, shear modulus G, Young's modulus Y, and Poisson's ratio υ have been estimated via the Voight–Reuss–Hill (VRH) approximation.[43] The bulk modulus B_0 was obtained through fitting the third-order Birch–Murnaghan equation of states. In addition, the formation enthalpy of these FeB_4 was estimated by the following equation: $\Delta H_f = E_{total}(FeB_4) - [E_{total}(Fe) + 4E_{total}(B)]$, where $E_{total}(FeB_4)$ is the obtained total energy for FeB_4 at equilibrium volume and $E_{total}(Fe)$ and $E_{total}(B)$ are the respective total energies of pure bcc Fe and the most stable allotrope of crystalline boron (α-B) at zero pressure.

3. RESULTS AND DISCUSSION

3.1. Structure and Feature. The optimized equilibrium lattice parameters, cell volumes per formula unit, densities, and relative total energies (ΔE) for all the considered structures of FeB_4 are listed in Table 1. Furthermore, ΔE values under high pressure are collected in Table SI and plotted in Figure SI of the Supporting Information. According to the calculated relative total energies, the relative stability order among all the investigated structures for FeB_4 is 58-FeB_4 > 12-FeB_4 > 71-FeB_4 > RuB_4–FeB_4 > 59-FeB_4 > 166-FeB_4 > 194-FeB_4 in the whole range of pressure, suggesting that the experimentally synthesized 58-FeB_4 is energetically more favorable than the others. Moreover, it is seen that the obtained lattice parameters and cell volumes for the 58-FeB_4 phase are in excellent agreement with the available experimental[31] and theoretical

dx.doi.org/10.1021/ic402913k | Inorg. Chem. 2014, 53, 3471−3479

Table 2. Elastic Constants C_{ij} (GPa) for All Considered FeB_4 with Various Different Structures and Available Theoretical Values

	C_{11}	C_{22}	C_{33}	C_{44}	C_{55}	C_{66}	C_{12}	C_{13}	C_{23}
58-FeB_4	379	761	466	226	152	233	136	143	144
theor.[a]	381	710	435	218	114	227	137	143	128
12-FeB_4	414	474	830	220	227	100	185	105	134
194-FeB_4	302		332	92		36	232	227	
71-FeB_4	484	954	536	217	208	170	53	144	117
59-FeB_4	355	335	264	105	211	149	4	32	19
166-FeB_4	252		321	156			4	−11	
RuB_4−FeB_4	500		963	221		153	197	209	

[a]Reference 31, VASP.

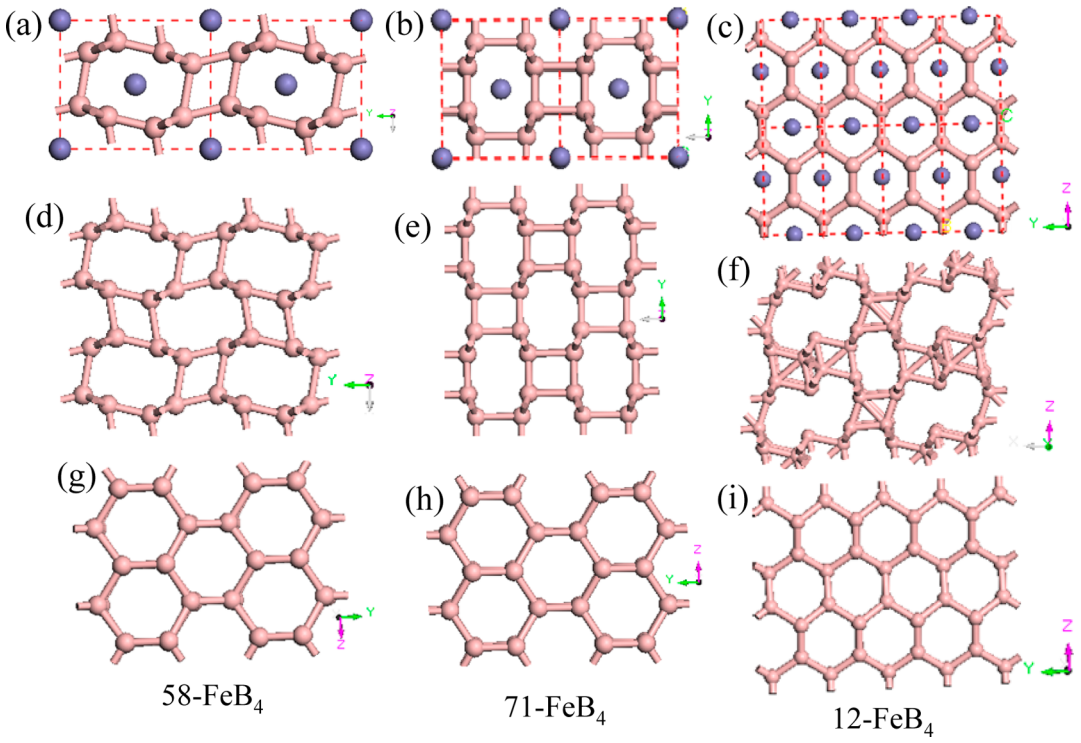

Figure 1. Crystal structures for 58-FeB_4 (a), 71-FeB_4 (b), 12-FeB_4 (c), and the corresponding structure of B layers appears (d−i) in these FeB_4 structures. Purple spheres represent Fe atoms, and pink spheres represent B atoms.

values[31,33,44] with deviations of less than 2%, verifying the reliability of the calculations here. For 12- and 71-FeB_4 phases, our calculations also agree well with previous theoretical predictions.[31] Unfortunately, there is not any available data to compare with our obtained results for the other phases. We hope that our results (lattice parameters and cell volumes) for these phases would provide a reference for further investigations in the future. In addition, the obtained elastic constants of the studied structures are tabulated in Table 2. It is found that these elastic constants satisfy the stability criteria,[41] indicating they are mechanically stable.

In order to systematically understand the structural features, the optimized structures of the considered FeB_4 are shown in Figures 1 and 2. It is illustrative to look at the evolution of the B network in the sequence of related structure types. From Figure 1, we found that 58-FeB_4, 71-FeB_4, and 12-FeB_4 all have a three-dimensional (3D) boron network in which the Fe atoms locate at the channels of the B network (Figure 1a−c, respectively). In the structure of 58-FeB_4, the honeycomb rings in the B layer (*ab* plane) (Figure 1d) with a larger degree of undulation are connected by the rhombus B ring. In 71-FeB_4, the honeycomb B rings are interconnected by rectangular boron (B_4) units which lie parallel with the layers along the *a* axis. The connecting sites in the B honeycomb locate at B−B bonds parallel to the *b* axis. As for 12-FeB_4, a similar scenario of connections between B layers happens. It can be seen clearly that these three FeB_4 compounds comprised of B_4 units are similar to tetragonal C_4, which has been predicted to be superhard.[40] Thus, we expect that these FeB_4 compounds may hold more outstanding mechanical properties. As can be seen from Figure 2a, 2b, and 2c, the 3D B network could not be found in the RuB_4−FeB_4, 59-FeB_4, and 166-FeB_4 structures. The B layers are comprised of two sublayers of honeycomb B rings (Figure 2e−g, respectively) and the Fe atoms along the *a* axis for the former and *b* axis for the later two. A connection between the B layers is absent due to the large distance between them (4.095 Å for RuB_4−FeB_4, 2.711 Å for 59-FeB_4, and 3.425 Å 166-FeB_4). However, two B sublayers are interconnected by short B−B bonds. These B−B covalent networks may contribute to their hardness.

3.2. Mechanical Properties. The mechanical stability is a necessary condition for the existence of a crystal. Accurate

dx.doi.org/10.1021/ic402913k | Inorg. Chem. 2014, 53, 3471−3479

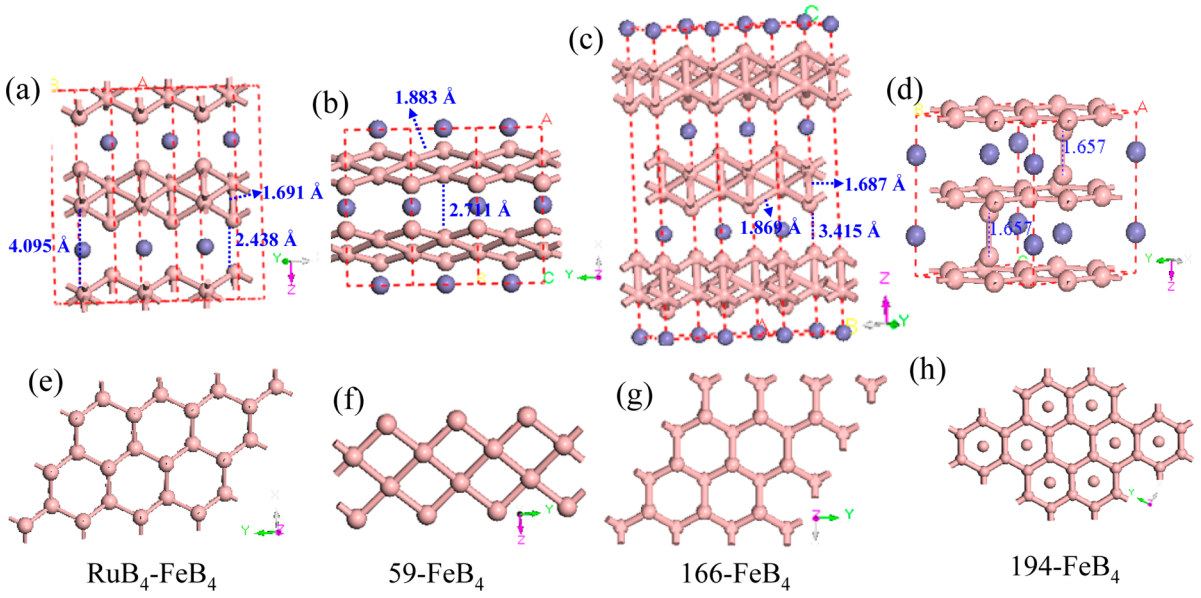

Figure 2. Crystal structures for RuB_4–FeB_4 (a), 59-FeB_4 (b), 166-FeB_4 (c), WB_4–FeB_4 (d), and the corresponding structure of B layers appears (e–h) in these FeB_4 structures. Purple and pink spheres represent Fe and B atoms, respectively.

Table 3. Calculated Bulk Modulus *B* (GPa), Shear Modulus *G* (GPa), Young's Modulus *Y* (GPa), *B*/*G*, Poisson's Ratio ν, Elastic Anisotropy Index A^U, and Formation Enthalpy ΔH_f (eV) for FeB_4

tetraboride	*B*	B_0	*G*	*Y*	*B*/*G*	ν	A^U	ΔH_f
58-FeB_4	263	267	194	467	1.36	0.20	0.45	−0.79
exp.[a]	253		177					
theor.[b]	265		198					
12-FeB_4	278	292	180	444	1.54	0.23	1.03	−0.73
194-FeB_4	248	261	56	156	4.43	0.26	1.17	1.78
71-FeB_4	235	257	222	507	1.06	0.14	0.03	−0.69
59-FeB_4	118	128	149	315	0.79	0.06	0.32	−0.54
166-FeB_4	87	94	142	276	0.61	−0.02	0.08	−0.40
RuB_4–FeB_4	344	352	202	507	1.70	0.25	0.43	−0.57

[a]Reference 32, experiment. [b]Reference 44, VASP.

elastic constants not only are helpful to understand the mechanical properties but also provide very useful information to estimate the hardness of a material. Therefore, the elastic constants of all the considered FeB_4 with various different structures were obtained using the strain–stress method and are tabulated in Table 2. As is seen in Table 2, the calculated elastic constants for 58-FeB_4 are in excellent agreement with the previous theoretical values.[31] The large values of C_{11}, C_{22}, and C_{33} for all FeB_4 phases indicate that they are extremely difficult to be compressed along the *a* axis, *b* axis, and *c* axis, respectively. Additionally, the calculated elastic constants (except C_{12} and C_{22}) of 71-FeB_4 are very close to those of 58-FeB_4, revealing that they have a very similar structure. It is worth noting that the extremely large C_{22} value (954 GPa) of 71-FeB_4 phase and C_{33} (963 GPa) of RuB_4–FeB_4 are comparable to C_{11} (1042 GPa) of diamond and C_{33} (1015 GPa) of ReB_2 as well as much greater than that of c-BN (773 GPa),[45,46] suggesting the extremely high incompressibility along the *b* and *c* axis, respectively. This large value of 71-FeB_4 may be attributed to the B_4 units in this structure, and this unit is similar to metastable tetragonal C_4 which has been predicted to be superhard.[40]

On the basis of the calculated elastic constants, the bulk modulus and shear modulus are determined by the Voiget–Reuss–Hill (VRH) approximation. The Young's modulus *Y* and Poisson's ratio ν are calculated by equations $Y = (9GB)/(3B + G)$ and $\nu = (3B - 2G)/[2(3B + G)]$, respectively. The obtained values of *B*, *G*, *Y*, and ν are listed in Table 3. It is clearly seen that the calculated *B* agrees well with the Birch–Murnaghan equation of states, demonstrating the good accuracy of our elastic calculations. In view of 58-FeB_4, all values of *B* (263 GPa) and *G* (194 GPa) agree well with the experimental data (253 and 177 GPa).[32] This gives us more confidence in the reliability of our selected computational method. In addition, Table 3 shows the calculated bulk modulus of all predicted phases. From Table 3 it is found that the RuB_4–FeB_4 phase has the largest bulk modulus (344 GPa), which is larger than those of superhard WB_4 (304 GPa)[17] and CrB_4,[33] indicating it may be grouped into an incompressible material. Compared to the bulk modulus, the shear modulus of a material quantifies the resistance to the shear deformation and is a better indicator of potential hardness. The 58-, 12-, 71-, 59-, and RuB_4–FeB_4 have maximum *G* values (194, 180, 222, 149, and 202 GPa, respectively) and minimum ν (0.20, 0.23, 0.14, 0.06, and 0.25, respectively), suggesting their strong directional bonding. Meanwhile, they also have large Young's modulus. Hence, the FeB_4 of these phases could be potentially hard materials. The ratio *B*/*G* is usually used to describe the ductility

dx.doi.org/10.1021/ic402913k | Inorg. Chem. 2014, 53, 3471–3479

or brittleness of a material. According to the Pugh criteria,[47] the ductile behavior is predicted when $B/G > 1.75$; otherwise, the material behaves in a brittle manner. In our case, all phases possess the brittle nature due to their B/G values being less than 1.75, with the exception of 194-FeB_4 (for which B/G = 4.43). As for majority of FeB_4 phases, the value of B is larger than that of G. Only one deviation from this tendency is 71-FeB_4, whose B is almost equal to G.

The elastic anisotropy of materials is an important implication in engineering science due to it is highly related occurrence of microcracks in materials. Here, A^U of the considered FeB_4 is estimated based on a new universal elastic index defined as $A^U = 5G^V/G^R + B^V/B^R - 6$ (for isotropic crystals $A^U = 0$; deviations of A^U from zero define the extent of crystal anisotropy),[48] where B and G represent the bulk and shear modulus and the superscripts V and R stand for the Voigt and Reuss approximations. The calculated A^U is collected in Table 3. It is noted that the 194-FeB_4 phase is significantly anisotropic, and the others also exhibit some anisotropy to a certain degree. However, 71- and 166-FeB_4 have a relatively strong isotropic character compared to their anisotropy, as revealed by their small A^U values approaching zero.

3.3. Formation Enthalpy. To gain deep insight into the thermodynamic stability of FeB_4 with various different structures, we calculated their formation enthalpies. The obtained results are listed in Table 3. A negative ΔH_f indicates a structure has thermodynamic stability with respect to the elemental constituents and vice versa. As shown in Table 3, the negative formation enthalpies of 58-, 12-, 71-, 59-, 166-, and RuB_4–FeB_4 suggest that these phases are thermodynamically stable and could be synthesized at ambient conditions. The formation enthalpies per atom (about −0.16 and −0.14 eV/atom, respectively) of 58- and 71-FeB_4 phases are in excellent agreement with previous theoretical values,[31,33,44] validating our methodology. Furthermore, it can be seen that the 58-FeB_4 phase has the smallest formation enthalpy among all considered phases, which demonstrated that it is the most thermodynamically stable against decomposition into mixtures of bcc-Fe and α-B. Meanwhile, the calculated difference in energies of the modeled phases relative to 58-FeB_4 also indicates that 58-FeB_4 is the most energetically stable. Moreover, the WB_4-type FeB_4 possesses a positive formation enthalpy of 1.78 eV, hinting that it is thermodynamically unstable. Thus, it will be not considered in our following discussion.

Extra pressure could enhance the thermodynamic stability or the reaction kinetics of a compound during its synthesis process, promoting its formation in the predicted configuration. Thus, we further calculated the formation enthalpy of FeB_4 under a pressure up to 100 GPa (Figure 3). From Figure 3 we can see that the stabilities of all FeB_4 with various structures are gradually enhanced as the pressure is increased, which suggests that the pressure is helpful to their stabilities. However, the formation enthalpy of 194-FeB_4 is still positive under the considered pressure range, indicating that much higher pressure is needed for its stability. For 58-FeB_4, the Fe + 4B constituent is always thermodynamically more favorable in the entire range of the pressure, suggesting that the synthesis route of pure Fe + nB is applicable. As for 59-FeB_4 and RuB_4–FeB_4, their formation enthalpies are almost equal to each other above 50 GPa, indicating that they have similar structure. This similarity is further verified by the differences in energies of them relative to 58-FeB_4 as a function of pressure (Figure SI, Supporting Information). In order to further understand the influence of

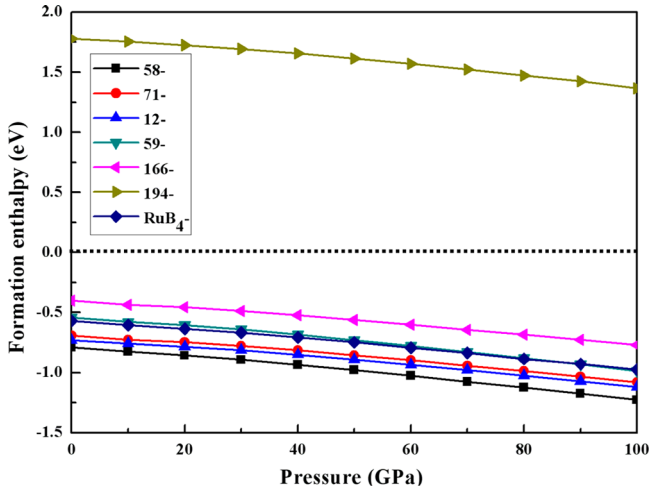

Figure 3. Relative formation enthalpy against pressure diagram for various FeB_4.

the different boron structure on the thermodynamic stability of crystals at pressure of 0–100 GPa, two polymorphs of boron α-B and γ-B were considered here. The calculated formation enthalpies for various different FeB_4 with respect to the Fe + 4α-B and Fe + 4γ-B reactants are presented in Figure 4. It is clearly seen that all FeB_4 crystals that dissociate into Fe + 4γ-B are thermodynamically more favorable.

Additionally, it is known that a phonon is a strict measure to check out dynamical stability. We thus carefully performed the phonon dispersion calculation within the finite displacement theory for all phases except 194-FeB_4. Our results indicate that 71-FeB_4 is dynamically instabile due to the occurrence of imaginary frequencies (Figure 5b), which is consistent with the result of Kolmogorov et al.[31] On the contrary, the absence of any imaginary phonon frequency in the whole Brillouin zone for 58-, 12-, 59-, 166-, and RuB_4–FeB_4 (Figure 5a, 5c, 5d, 5e and 5f, respectively) gives direct proof of their dynamical stabilities at ambient condition.

3.4. Electronic Structures. To explore the underlying origin of the stability, mechanical property, and chemical bonding of FeB_4 with various different structures, the total and partial density of states (DOS) of 58-, 71-, 12-, 166-, 59-, and RuB_4–FeB_4 are calculated at zero pressure. As displayed in Figure 6, all calculated phases exhibit metallic behavior due to the finite electron DOS at the Fermi level, which is mainly attributed to the B-p and Fe-d states. Therefore, they may be used as hard conductors. From the partial DOS, it is seen that the peaks in the range from about −4 to 1.7 eV originate mostly from the B-p state, and the Fe-d state has only a small contribution. The states, near the Fermi level (−4 to 1.7 eV), mainly originate from Fe-d orbitals. Moreover, we find that the typical feature of these FeB_4 is that there is a deep valley at the Fermi level, except for those of 166- and RuB_4–FeB_4, namely, the pseudogap at the Fermi level is the borderline between the bonding and the antibonding states.[49] The presence of this pseudogap will surely increase structural stabilities of these phases, which also implies strongly covalent bonding Fe–B exists. More importantly, the partial DOS profiles overlap for these phases, indicating hybridization between Fe-d and B-p; thus, the strong covalent bonding character emerges. The strong covalent bonding would be beneficial to their high bulk and shear modulus. However, one observes an intriguing bonding situation in DOS of 166- and RuB_4–FeB_4, that is, Fe

dx.doi.org/10.1021/ic402913k | Inorg. Chem. 2014, 53, 3471–3479

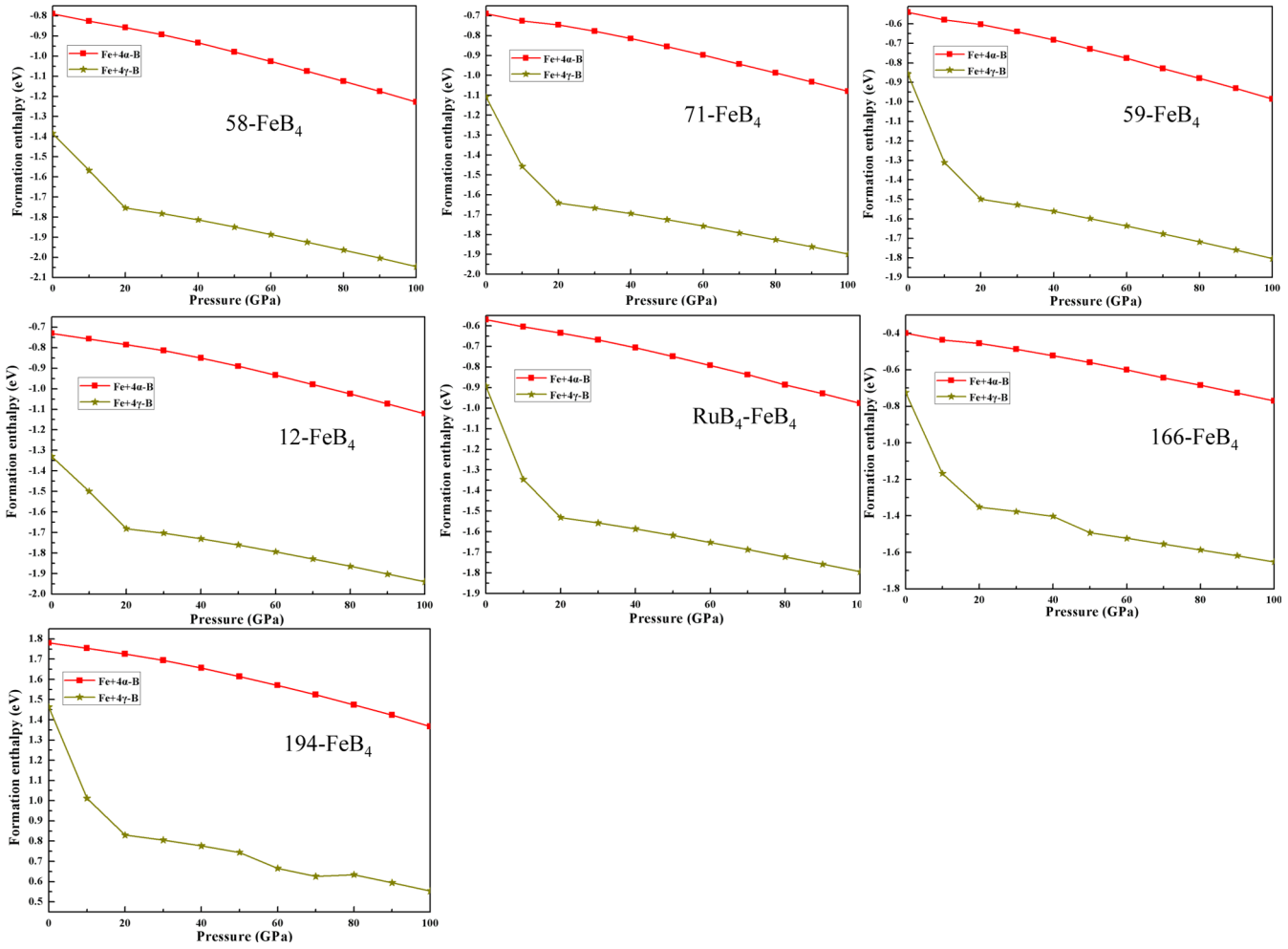

Figure 4. Relative formation enthalpy of various FeB_4 with respect to the pure Fe and α-B (or γ-B) reactants under 0−100 GPa.

and B form only weak covalent bonds as suggested by the mismatching Fe-d and B-p curve shape. In order to further explore whether the metallic behavior of all phases relate to the approach used or not, we calculated the total and partial DOS of those FeB_4 structures using the local density approximation (LDA). The results are presented in Figure SII, Supporting Information. From Figure SII, Supporting Information, it is found that all the phases also exhibit metallic behavior, namely, their metallic behavior does not relate to the approach used.

3.5. Hardness. Even though a correlation has been observed between hardness and bulk modulus, shear modulus, Poisson's ratio, B/G ratio, as well as strong covalent bonding, it is widely accepted that hardness is different from the bulk and shear modulus. Therefore, the hardness of our considered crystal structures with partial metallic bond is calculated based on the semiempirical model,[50,51] which seems to be of great interest. For estimation of the Vickers hardness (H_v) on multicomponent systems, their hardness is expressed as

$$H_v(\mathrm{GPa}) = [\prod^{\mu} (H_v^{\mu})^{n^{\mu}}]^{1/\sum n^{\mu}} \quad (1)$$

Here $H_v(\mathrm{GPa}) = 699 P v_b^{-5/3} \exp(-3005 f_m^{1.553})$ in which allowance for metallicity of bonds in the crystal structure is made. This method has been tested successfully by our group[52] using a group of transition metal carbides and nitrides as an example. The results show that the calculated Vickers hardness values agree well with the experimental data. In this equation, a factor of metallicity $f_m = 0.026N(E_F)/n_e$ ($N(E_F)$) is the density of electronic states at the Fermi level, n_e is the total number of valence electrons in the unit cell, P is Mulliken population, and ν_b is the volume of a bond. The following equation was used to calculate ν_b

$$v_b^{\mu} = (d^{\mu})^3 / \sum [(d^{\nu})^3 N_b^{\nu}] \quad (2)$$

Thus, using the above expression 1, we predicted the Vickers hardness for some of our considered tetraborides. The calculated bond parameter and Vickers hardness are presented in Table 4. It is found that the FeB_4 with OsB_4-type structure has exceptionally large Vickers hardness (48.1 GPa), well exceeding the superhardness threshold of 40 GPa. This indicates that 59-FeB_4 is a superhard material. The 58-FeB_4 and 71-FeB_4 with similar structure also possess large hardness (34.2 and 31.7 GPa, respectively) due to the unusual rectangular B_4 units, suggesting their highly incompressible nature. Unfortunately, the latter is unstable as revealed by the above discussion on phonon dispersion. In addition, our calculated result of 58-FeB_4 agrees with Niu's result (about 27.9 GPa)[33] based on Chen's model[53] and the theoretical result (11.7−32.2 GPa) of Zhang group[44] but is lower than the experimental value of 65(5) GPa.[32] The deviation between our predicted value and the experimentally measured one may be related to the fact that the experimentally measured hardness is the nanoindentation hardness which depends on the loads and

dx.doi.org/10.1021/ic402913k | Inorg. Chem. 2014, 53, 3471−3479

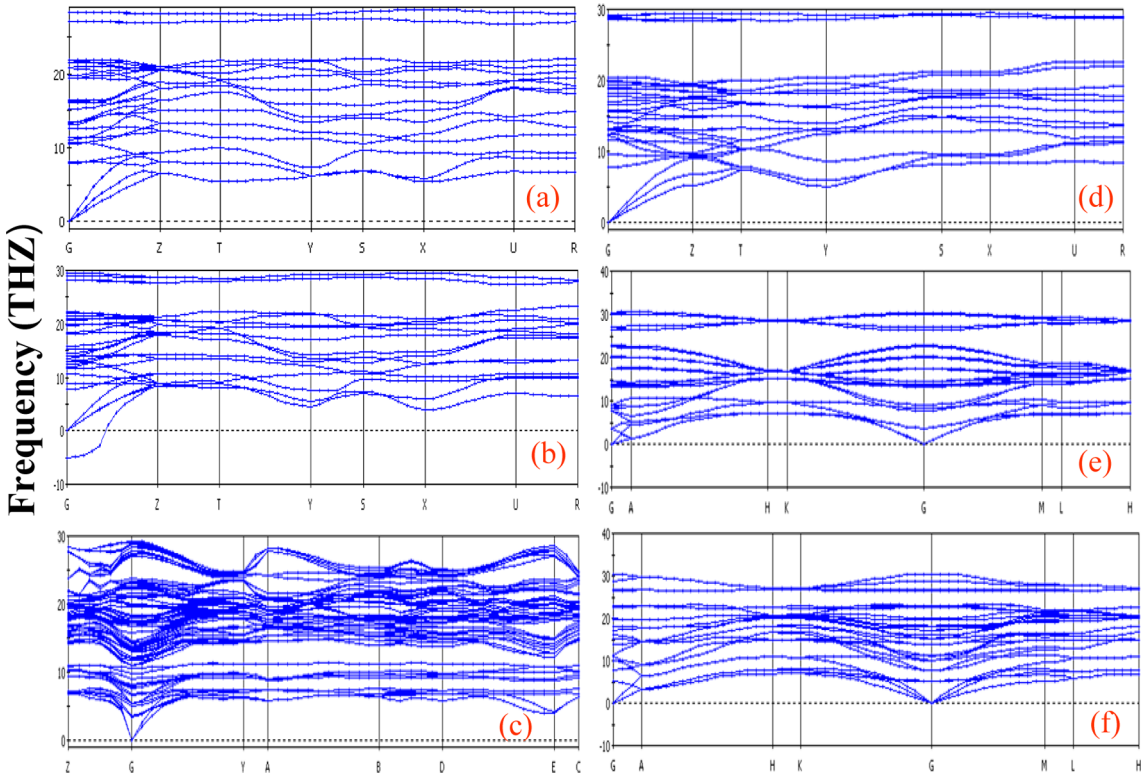

Figure 5. Phonon dispersion for 58-FeB_4 (a), 71-FeB_4 (b), 12-FeB_4 (c), 59-FeB_4 (d), 166-FeB_4 (e), and RuB_4–FeB_4 (f).

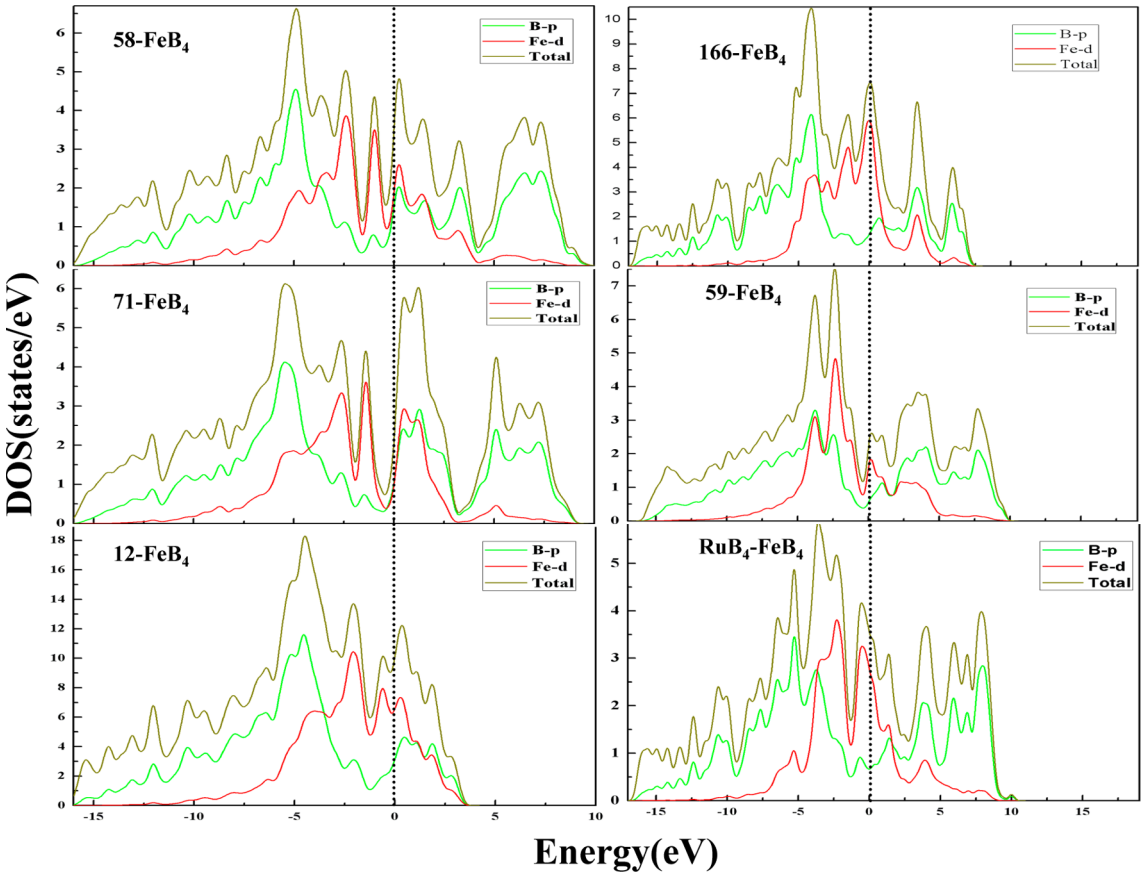

Figure 6. Total and partial density of states for 58-FeB_4, 71-FeB_4, 12-FeB_4, 59-FeB_4, 166-FeB_4, and RuB_4–FeB_4 with stable structure.

dx.doi.org/10.1021/ic402913k | Inorg. Chem. 2014, 53, 3471−3479

Table 4. Calculated Bond Parameters and Vickers Hardness for Some FeB_4

	bond	d	v_b	P	$f_m(10^{-3})$	H_v		bond	d	v_b	P	$f_m(10^{-3})$	H_v
58-FeB_4	B−B	1.695	3.996	0.91	0	34.2	12-FeB_4	B−B	1.693	3.009	0.87	0	29.6
	B−B	1.832	5.045	1.55	0	27.9[a]		B−B	1.693	3.009	0.53	0	
	B−B	1.875	5.049	0.42	0	11.7−32.2[b]		B−B	1.700	3.047	0.89	0	
	B−B	1.984	6.408	0.24	0			B−B	1.809	3.671	0.54	0	
71-FeB_4	B−B	1.676	4.758	1.01	0	31.7		B−B	1.809	3.671	1.59	0	
	B−B	1.824	6.133	1.56	0			B−B	1.822	3.751	1.53	0	
	B−B	1.908	7.020	0.42	0			B−B	1.872	4.068	1.14	0	
59-FeB_4	B−B	1.668	3.116	0.59	0	48.1		B−B	1.884	4.147	0.71	0	
	B−B	1.883	5.061	0.87	0			B−B	1.891	4.193	0.42	0	
	B−B	1.892	1.441	0.60	0			B−B	1.894	4.213	0.42	0	
	B−B	1.979	1.577	0.72	0			B−B	1.951	4.605	0.29	0	
	B−B	1.997	1.605	0.59	0			B−B	1.988	4.872	0.31	0	
	B−B	2.044	7.027	0.17	0			Fe−B	2.060	5.421	0.13	8.612	
RuB_4−FeB_4	B−B	1.691	2.809	0.27	0	25.3		Fe−B	2.122	5.926	0.34	8.612	
	B−B	1.850	3.679	1.62	0		166-FeB_4	B−B	1.687	2.326	0.28	0	20.6
	B−B	1.866	3.775	1.15	0			B−B	1.843	3.033	1.65	0	
	B−B	2.438	8.419	0.07	0			B−B	1.869	3.164	1.12	0	
	Fe−B	2.054	5.035	0.29	3.591			B−B	2.992	12.979	0.02	0	
								Fe−B	2.071	4.304	0.34	7.668	

[b]Reference 33 [a]Reference 44, VASP.

the maximum indentation depth. In 58-, 71- and 59-FeB_4, all Fe−B bonds are antibonding states; hence, these Fe−B bonds are not considered. Compared with 58-FeB_4, the second stable 12-FeB_4 possesses a smaller hardness of 29.6 GPa. As for 166-FeB_4 and RuB_4−FeB_4, although both structures have four B−B bonds and one Fe−B bond, the hardness of RuB_4−FeB_4 is larger than that of 166-FeB_4 due to the 3D honeycomb B network and strong B−B covalent bond in the former (as suggested by P in Table 4). This fact indicates that the atomic configuration and strong B−B covalent bond are responsible for the high hardness.

4. CONCLUSIONS

In summary, we established a comprehensive understanding of the structural features, mechanical properties, formation enthalpies, electronic structures, and hardness of FeB_4 with various different structures by first-principle techniques. All the results are summarized as follows.

(1) The orthorhombic *Pnnm* structure is the most stable phase among all calculated FeB_4. Additionally, the other four predicted new dynamically stable phases (monoclinic $C2/m$, orthorhombic *Pmmn*, trigonal $R\bar{3}m$, and hexagonal $P6_3/mmc$) have been identified. Their mechanical and thermodynamic stability are verfied by calculating elastic constants, formation enthalpy, and phonon dispersion. It is found that all FeB_4 phases are stabilized further under pressure. Above a pressure of about 50 GPa, the formation enthalpy of *Pmmn* is almost equal to that of $P6_3/mmc$ phase.

(2) Analysis on density of states shows that all calculated phases exhibit metallic behavior which does not relate to the approach used. Also, their chemical bond is mainly a strong covalent bond nature with partial metallic contributions.

(3) The Vickers hardness values, calculated by a semi-empirical method in which the role of metallic contributions is considered, demonstrated that the OsB_4-structured FeB_4 is a superhard material with an exceptionally large hardness of 48.1 GPa. This large value well exceeds the superhardness threshold of 40 GPa, while the experimentally synthesized *Pnnm* phase and the other three predicted dynamically stable phases are all hard materials. Moreover, it is found that the atomic configuration and strong B−B covalent bond are responsible fot their high hardness.

■ ASSOCIATED CONTENT

Ⓢ Supporting Information

The relative total energies between the most stable 58-FeB_4 and other phases under high pressure are listed in Table SI and presented in Figure SI. In addition, the total and partial density of states (DOS) of FeB_4 with various different structures using the local density approximation (LDA) is shown in Figure SII. This material is available free of charge via the Internet at http://pubs.acs.org.

■ AUTHOR INFORMATION

Corresponding Author

*Phone/fax: +86 28 85405515. E-mail: scu_kuang@163.com.

Notes

The authors declare no competing financial interest.

■ ACKNOWLEDGMENTS

The authors are grateful to the National Natural Science Foundation of China (Nos. 11274235 and 11104190) and the Doctoral Education Fund of Education Ministry of China (Nos. 20100181110086 and 20110181120112).

■ REFERENCES

(1) Vepre, S. *J. Vac. Sci. Technol. A* **1999**, *17*, 2401.
(2) Sproul, W. D. *Science* **1996**, *273*, 889.
(3) Haines, J.; Leger, J. M.; Bocquillon, G. *Ann. Rev. Mater. Res.* **2001**, *31*, 1.
(4) He, D.; Zhao, Y.; Daemen, L.; Qian, J.; Shen, T. D.; Zerda, T. W. *Appl. Phys. Lett.* **2002**, *81*, 643.
(5) Solozhenko, V. L.; Kurakevych, O. O.; Andrault, D.; Godec, Y. L.; Mezouar, M. *Phys. Rev. Lett.* **2009**, *102*, 015506.

(6) Gregoryanz, E.; Sanloup, C.; Somayazulu, M.; Badro, J.; Fiquet, G.; Mao, H. K.; Hemley, R. *J. Nat. Mater.* **2004**, *3*, 294.
(7) Cumberland, R. W.; Weinberger, M. B.; Gilman, J. J.; Tolbert, S. H.; Kaner, R. B. *J. Am. Chem. Soc.* **2005**, *127*, 7264.
(8) Chung, H. Y.; Weinberger, M. B.; Levine, J. B.; Yang, J. M.; Tolbert, S. H.; Kaner, R. B. *Science* **2007**, *316*, 436.
(9) Dubrovinskaja, N.; Dubrovinsky, L.; Solozhenko, V. L. *Science* **2007**, *318*, 1550c.
(10) Zhang, X. H.; Hilmas, G. E.; Fahrenholtz, W. G. *Mater. Lett.* **2008**, *62*, 4251.
(11) Tse, J. S.; Klug, D. D.; Uehara, K.; Li, Z. Q.; Hains, J.; Léger, J. M. *Phys. Rev. B* **2000**, *61*, 10029.
(12) Kaner, R. B.; Gilman, J. J.; Tolbert, S. H. *Science* **2005**, *308*, 1268.
(13) Yang, J.; Sun, H.; Chen, C. F. *J. Am. Chem. Soc.* **2008**, *130*, 7200.
(14) Zhang, R. F.; Legut, D.; Niewa, R.; Argon, A. S.; Veprek, S. *Phys. Rev. B* **2010**, *82*, 104104.
(15) Friedrich, A.; Winkler, B.; Bayarjargal, L.; Morgenroth, W.; Juarez-Arellano, E. A.; Milman, V.; Refson, K.; Kunz, M.; Chen, K. *Phys. Rev. Lett.* **2010**, *105*, 085504.
(16) Zhang, R. F.; Lin, Z. J.; Mao, H. K.; Zhao, Y. S. *Phys. Rev. B* **2011**, *83*, 060101.
(17) Gu, Q. F.; Krauss, G.; Steurer, W. *Adv. Mater.* **2008**, *20*, 3620.
(18) Wang, M.; Li, Y. W.; Cui, T.; Ma, Y. M.; Zou, G. T. *Appl. Phys. Lett.* **2008**, *93*, 101905.
(19) Li, Q.; Zhou, D.; Zheng, W. T.; Ma, Y. M.; Chen, C. F. *Phys. Rev. Lett.* **2013**, *110*, 136403.
(20) Mohammadi, R.; Lech, A. T.; Xie, M.; Eeaver, B. E.; Yeung, M. T.; Tolbert, S. H.; Kaner, R. B. *Proc. Natl. Acad. Sci. U.S.A.* **2011**, *108*, 10958.
(21) Wang, M. G.; Yan, H. Y.; Zhang, G. T.; Wang, H. *J. Phys. Chem. C* **2012**, *116*, 4293.
(22) Balani, K.; Agarwala, A.; Dahotre, N. B. *J. Appl. Phys.* **2006**, *99*, 044904.
(23) Moorjani, K.; Poehler, T. O.; Satkiewicz, F. G. *J. Appl. Phys.* **1985**, *57*, 3444.
(24) Voroshnin, L. G.; Lyakhovich, L. S.; Panich, G. G.; Protasevich, G. F. *Met. Sci. Heat Treat.* **1970**, *12*, 732.
(25) Burdett, J. K.; Canadell, E.; Miller, G. J. *J. Am. Chem. Soc.* **1986**, *108*, 6561.
(26) Burdett, J. K.; Canadell, E. *Inorg. Chem.* **1988**, *27*, 4437.
(27) Mohn, P.; Pettifor, D. G. *J. Phys. C: Solid State Phys.* **1988**, *21*, 2829.
(28) Mohn, P. *J. Phys. C: Solid State Phys.* **1988**, *21*, 2841.
(29) Ching, W. Y.; Xu, Y. N.; Harmon, B. N.; Ye, J.; Leung, T. C. *Phys. Rev. B* **1990**, *42*, 4460.
(30) Ohodnicki, P. R., Jr.; Cates, N. C.; Laughlin, D. E.; McHenry, M. E.; Widom, M. *Phys. Rev. B* **2008**, *78*, 144414.
(31) Kolmogorov, A. N.; Shah, S.; Margine, E. R.; Bialon, A. F.; Hammerschmidt, T.; Drautz, R. *Phys. Rev. Lett.* **2010**, *105*, 217003.
(32) Gou, H. Y.; Dubrovinskaia, N.; Bykova, E.; Tsirlin, A. A.; Kasinathan, D.; Richter, A.; Merlini, M.; Hanfland, M.; Abakumov, A. M.; Batuk, D.; Tendeloo, G. V.; Nakajima, Y.; Kolmogorov, A. N.; Dubrovinsky, L. *Phys. Rev. Lett.* **2013**, *111*, 157002.
(33) Niu, H. Y.; Wang, J. Q.; Chen, X. -Q.; Li, D. Z.; Li, Y. Y.; Lazar, P.; Podloucky, R.; Kolmogorov, A. N. *Phys. Rev. B* **2012**, *85*, 144116.
(34) Ramans, P. A.; Krug, M. P. *Acta Crystallogr.* **1966**, *20*, 313.
(35) Wang, Y. C.; Lv, J.; Zhu, L.; Ma, Y. M. *Phys. Rev. B: Condens. Matter Mater. Phys.* **2010**, *82*, 094116.
(36) Wang, B.; Wang, D. Y.; Wang, Y. X. *J. Alloys Compd.* **2013**, *573*, 20.
(37) Zhang, M. G.; Wang, H.; Wang, H. B.; Cui, T.; Ma, Y. M. *J. Phys. Chem. C* **2010**, *114*, 6722.
(38) *MATERIALS STUDIO*, version 4.1; Accelrys Inc.: San Diego, CA, 2006.
(39) Perdew, J. P.; Burke, K.; Ernzerhof, M. *Phys. Rev. Lett.* **1996**, *77*, 3865.
(40) Vanderbilt, D. *Phys. Rev. B.* **1990**, *41*, 7892.
(41) Monkhorst, H. J.; Pack, J. D. *Phys. Rev. B* **1976**, *13*, 5188.
(42) Wu, Z. J.; Zhao, E. J.; Xiang, H. P.; Hao, X. F.; Liu, X. J.; Meng, J. *Phys. Rev. B* **2007**, *76*, 054115.
(43) Hill, R. *Proc. Phys. Soc. A* **1952**, *65*, 349.
(44) Zhang, M.; Lu, M. H.; Du, Y. H.; Gao, L. L.; Lu, C.; Liu, H. Y. http://arxiv.org/abs/1311.4006.
(45) Chen, Z. Y.; Xiang, H. J.; Yang, J.; Hou, J. G.; Zhu, Q. S. *Phys. Rev. B* **2006**, *74*, 012102.
(46) Wang, Y. X. *Appl. Phys. Lett.* **2007**, *91*, 101904.
(47) Pugh, S. F. *Philos. Mag.* **1954**, *45*, 823.
(48) Ranganathan, S. I.; Ostoja-Starzewski, M. *Phys. Rev. Lett.* **2008**, *101*, 055504.
(49) Vajeeston, P.; Ravindran, P.; Ravi, C.; Asokamani, R. *Phys. Rev. B* **2001**, *63*, 045115.
(50) Andersson, S.; Lundstroem, T. *Acta Chem. Scand.* **1968**, *22*, 3103.
(51) Gao, F. M.; He, J. L.; Wu, E. D.; Liu, S. M.; Yu, D. L.; Li, D. C.; Zhang, S. Y.; Tian, Y. J. *Phys. Rev. Lett.* **2003**, *91*, 015502.
(52) Zhong, M. M.; Kuang, X. Y.; Wang, Z. H.; Shao, P.; Ding, L. P.; Huang, X. F. *J. Alloys Compd.* **2013**, *581*, 206.
(53) Gao, F. M. *Phys. Rev. B* **2006**, *73*, 132104.